

Ensemble-based gradient inference for particle methods in optimization and sampling

Claudia Schillings, Claudia Totzeck and Philipp Wacker

October 3, 2022

Abstract

We propose an approach based on function evaluations and Bayesian inference to extract higher-order differential information of objective functions from a given ensemble of particles. Pointwise evaluation $\{V(x^i)\}_i$ of some potential V in an ensemble $\{x^i\}_i$ contains implicit information about first or higher order derivatives, which can be made explicit with little computational effort (ensemble-based gradient inference – EGI). We suggest to use this information for the improvement of established ensemble-based numerical methods for optimization and sampling such as Consensus-based optimization and Langevin-based samplers. Numerical studies indicate that the augmented algorithms are often superior to their gradient-free variants, in particular the augmented methods help the ensembles to escape their initial domain, to explore multimodal, non-Gaussian settings and to speed up the collapse at the end of optimization dynamics. The code for the numerical examples in this manuscript can be found in the paper’s Github repository¹

1 Introduction

Global optimization of nonconvex objective functions and sampling from nonstandard distributions are widespread applications in industry, finance and other disciplines. Although the problems read very simple, and there is a variety of algorithms available, it is still very challenging to design well-performing algorithms and to prove their convergence. We motivate both the optimization and sampling problem via the inverse setting, where the goal is to identify unknown parameters $x \in \mathbb{R}^d$ from noisy observations

$$y = G(x) + \eta, \quad (1.1)$$

with $G : \mathbb{R}^d \rightarrow \mathbb{R}^k$ denoting the parameter-to-observation map and η being the noise. Under suitable assumptions on G and η , application of Bayes’ theorem gives as solution of the (Bayesian) inverse problem the following characterization of the posterior distribution

$$\frac{d\mu(x)}{d\lambda(x)} \propto \exp(-V(x)) \quad (1.2)$$

w.r. to the Lebesgue measure λ , where V denotes a regularized potential. The aim of sampling methods is then to generate samples (approximately) distributed according to the

¹<https://github.com/MercuryBench/ensemble-based-gradient.git>

posterior distribution. The connection to the optimization setting is via the maximum-a-posteriori (MAP) estimate (assuming the unique existence) given by

$$x^* = \arg \max_x \exp(-V(x)) = \arg \min_x V(x). \quad (1.3)$$

The Bayesian approach to inverse problems has become very popular over the last decades and there has been a lot of research effort towards efficient methods, in particular gradient-free methods in order to allow the use of black-box solvers for the underlying forward problem. Kalman-Wasserstein flows have been the basis to design various efficient, gradient-free samplers, e.g. Ensemble Kalman Sampler Garbuno-Inigo et al. (2020a); Nüsken and Reich (2019), Affine Invariant Interacting Langevin Dynamics Garbuno-Inigo et al. (2020b). Also in the optimization setting, gradient free methods such as Consensus-based optimization method (CBO) and Ensemble Kalman Inversion (EKI) have become very popular, see e.g. Blömker et al. (2019); Carrillo et al. (2018, 2021); Schillings and Stuart (2017); Totzeck (2022) and the references therein. These methods have in common that they rely on an ensemble of particles, which is transformed into posterior samples or concentrates around the minimizer in the limit 'time to infinity'. We will show in the following that the ensemble itself can be used to efficiently approximate derivative information (without any further evaluations of the forward problem). In order to do so, we will formulate the approximation of derivative information as an inverse problem and extract the information from given function evaluations. To demonstrate the potential of the simultaneous estimation of the derivative information and parameter estimation, we consider the ensemble based gradient augmentation of the following state-of-the art optimization and sampling methods:

- Consensus-based optimization (CBO)
- Ensemble Langevin sampler (LS)
- Metropolis-adjusted Langevin algorithm (MALA)
- Affine invariant interacting Langevin dynamics for Bayesian inference (ALDI) and Ensemble Kalman sampler (EKS).

In order to keep the presentation self-contained and for later reference we review the methods in the following.

1.1 Review of existing computational methods

We consider a potential V as described above which may be the negative logdensity of some Bayesian posterior measure, or just a function we want to minimize. We will call the task of finding the minimal value of V (if it exists) the *optimization task*, and the task of constructing samples from the measure with unnormalized Lebesgue-density $\exp(-V)$ will be called the *sampling task*.

CBO (for optimization) The consensus-based optimization (CBO) method Carrillo et al. (2018); Pinnau et al. (2017) describes the collective dynamical behavior of an ensemble of particles exploring the state space experiencing some diffusive behaviour and finally collapsing onto a joint weighted ensemble mean, which is by construction an approximation of the minimizer of V . Given a measure $\rho \in \mathcal{M}(\mathbb{R}^d)$ we define the weighted mean of ρ as

$$\mathbf{m}_\beta(\rho) := \frac{\int x \exp(-\beta V(x)) \, \mathrm{d}\rho(x)}{\int \exp(-\beta V(x)) \, \mathrm{d}\rho(x)}. \quad (1.4)$$

This definition of weighted mean is motivated by the Laplace principle Pinnau et al. (2017). Indeed, assuming that V admits a unique global minimizer, it can be shown that for $\beta \rightarrow \infty$, $\mathfrak{m}_\beta(\rho)$ tends to the $\arg \min_{x \in \text{supp } \rho} V(x)$.

The CBO dynamics combines exploration of the landscape given by V with aggregation of the ensemble around $\mathfrak{m}_\beta(\rho)$. More succinctly, it follows the following system of stochastic differential equations (SDEs), where $\rho := \sum_{i=1}^J \delta_{x^i}$.

$$dx^i = -\lambda(x^i - \mathfrak{m}_\beta(\rho)) dt + \sigma |x^i - \mathfrak{m}_\beta(\rho)| dW_t^i, \quad i = 1, \dots, J \quad (1.5)$$

with initial conditions $x_0^i \sim \mathcal{P}_2(\mathbb{R}^d)$ drawn independently. It is important to note that both the drift and the diffusion part of the dynamics scale with the distance $|x^i - \mathfrak{m}_\beta(\rho)|$. On the one hand this allows for collapse at $\mathfrak{m}_\beta(\rho)$ which is important for optimization tasks. On the other hand, the dynamics slows down as the ensemble variance becomes small.

We will call the algorithm corresponding to (1.5) “vanilla CBO” and in case the componentwise noise modification of Carrillo et al. (2018) is used, we will specify this as “component-wise noise vanilla CBO”. In Pinnau et al. (2017) the Consensus-based optimization method (CBO) was proposed as alternative to heuristic gradient-free particle optimization methods such as evolutionary or genetic algorithms and simulated annealing (Back, 1996; Simon, 2013; van Laarhoven and Aarts, 1987) with the intention to prove convergence for the corresponding mean-field dynamics (Carrillo et al., 2021). Based on these publications a variety of researchers from stochastic analysis (Huang and Qiu, 2022; Kalise et al., 2022), PDE analysis (Fornasier et al., 2021b, 2022) found ways to relax assumptions, give further insight in the internal process of the method (Fornasier et al., 2021b), open the class of applications like constraint problems (Fornasier et al., 2020, 2021a; Ha et al., 2022), machine learning (Carrillo et al., 2021), multiobjective problems (Borghi et al., 2022; Klamroth et al., 2022) and sampling (Carrillo et al., 2022b). Others aim to make the algorithm more reliable (Totzeck and Wolfram, 2020). As the original method with minimal dynamics is fairly understood, there are mainly two paths to go, either improve the method itself or use the established ideas to prove convergence results for other well-known optimization dynamics, see for example (Grassi and Pareschi, 2021; Huang, 2021) for Particle Swarm Optimization.

Langevin dynamics and MALA (for sampling) A well-known sampling dynamics is given by the (overdamped) Langevin equation, cp. Yang et al. (2019) for a recent overview for the connection of Langevin dynamics and Markov chain Monte Carlo (MCMC) methods. Given a symmetrical and positive definite matrix M , the (overdamped) Langevin equation preconditioned by M models a particle subject to the influence of the potential V :

$$dx_t = -M \nabla V(x_t) dt + \sqrt{2M^{1/2}} dW_t. \quad (1.6)$$

It can be shown that the invariant measure of this stochastic differential equation is equal to μ , i.e. the target measure μ with unnormalized Lebesgue-density $\exp(-V)$ Garbuno-Inigo et al. (2020b); Jordan et al. (1998). In applications the gradient of V may be expensive to compute or simply not available. It is therefore of interest to construct a surrogate model with a gradient approximation.

ALDI and EKS Another recent ensemble-based method with pointwise function evaluations is the gradient-free ALDI sampler Garbuno-Inigo et al. (2020b). It performs an implicit

approximation to the gradient of the loglikelihood. There is a close relationship between ALDI and the Ensemble Kalman sampler (EKS) Garbuno-Inigo et al. (2020a); Nüsken and Reich (2019) which is an efficient gradient-free interacting particle sampler originating from the Ensemble Kalman filter. EKS can be applied if the negative logdensity of ρ can be written in the form $V(x) = \frac{1}{2}\|y - A(x)\|_{\Gamma}^2 + \frac{1}{2}\|x - \mu_0\|_{\Sigma_0}^2$, which is typical for a Bayesian statistical problem. In this special case, the gradient-free ALDI is the coupled system of SDEs given by

$$\begin{aligned} dx_t^i = & -\{D(X_t)\Gamma^{-1}(A(x_t^i) - y) + C(X_t)\Sigma_0^{-1}(x_t^i - \mu_0)\} dt \\ & + \frac{d+1}{J}(x_t^i - \bar{x}_t) dt + \sqrt{2}C(X_t)^{\frac{1}{2}} dW_t^i \end{aligned} \quad (1.7)$$

where d is the dimension of the space and

$$\begin{aligned} C(X) &= \frac{1}{N} \sum_{j=1}^N (x^j - \bar{x}) \otimes (x^j - \bar{x}) \\ D(X) &= \frac{1}{N} \sum_{j=1}^N (x^j - \bar{x}) \otimes (A(x^j) - \bar{A}), \quad \bar{A} = \frac{1}{N} \sum_{j=1}^N A(x^j) \end{aligned} \quad (1.8)$$

with initial conditions analogous to the methods above. If A is a linear map, samples from ρ are provable accurately generated. One of its main strengths stems from the fact that the Ensemble Kalman method constructs a covariance-preconditioned approximation to the gradient: Note that if $V(x) = \frac{1}{2}\|A(x) - y\|_{\Gamma}^2$ and A linear, then

$$\begin{aligned} C(X) \cdot \nabla V(x^i) &= \frac{1}{N} \sum_{j=1}^N (x^j - \bar{x}) \langle x^j - \bar{x}, \nabla V(x^i) \rangle \\ &= \frac{1}{N} \sum_{j=1}^N (x^j - \bar{x}) \langle x^j - \bar{x}, A^T \Gamma^{-1}(Ax^i - y) \rangle \\ &= \frac{1}{N} \sum_{j=1}^N (x^j - \bar{x}) \langle A(x^j) - A(\bar{x}), \Gamma^{-1}(Ax^i - y) \rangle \\ &= D(X) \cdot \Gamma^{-1}(A(x^i) - y). \end{aligned}$$

For A linear, the approximation is exact. In fact, in the linear regime (1.7) corresponds to

$$dx_t^i = -C(X) \cdot \nabla V(x_t^i) dt + \frac{d+1}{J}(x_t^i - \bar{x}_t) dt + \sqrt{2}C(X_t)^{\frac{1}{2}} dW_t^i,$$

which is an overdamped Langevin equation with a correction term ensuring the affine invariance of the resulting scheme Garbuno-Inigo et al. (2020b).

1.2 Main idea and contributions of the paper

We argue that tracking an ensemble of particles $\{x^i\}_{i=1}^J$ with pointwise evaluations $\{V(x^i)\}_{i=1}^J$ of some potential function V carries implicit gradient (and higher-order differential) information which can be converted into explicit information basically “for free”, via an often

negligible cost of solving one linear equation system. This can and should be leveraged in various optimization and sampling tasks:

The CBO algorithm for optimization is completely gradient-agnostic and can benefit from incorporation of gradient information via EGI in order to speed up local convergence (“better convergence to minima”) and improve overall performance (“convergence to better minima”).

Langevin dynamics and MALA in its original form need explicit gradient information. By managing a full ensemble instead of just one particle and thereby providing approximated gradient information for each member of the ensemble via EGI, we can run approximated Langevin dynamics and MALA without the need for an explicit gradient functional.

EKS and ALDI utilize a powerful property of the empirical covariance of an ensemble in order to compute a preconditioned gradient without the need for any additional computation. This allows us to sample very efficiently from a Bayesian posterior. Unfortunately, this is an approximation that holds only in the linear, Gaussian setting. With EGI, we can obtain a better approximation of the gradient, allowing for construction of non-Gaussian posterior samples.

Summarized, we present, motivate, and test the following novel algorithms.

- **EGI**: Gradient approximation from ensemble point evaluation (as a general method)
- **EGI-CBO**: CBO augmented by gradient information
- **EGI-LS**: Coupled Langevin dynamics with approximated gradient information
- **EGI-MALA**: Coupled MALA dynamics with approximated gradient information
- **EGI-ALDI**: Gradient-free ALDI with approximated gradients, with some variants

The rest of the article is structured as follows: Section 2 describes how pointwise evaluation of some function V evaluated in an ensemble $\{x^i\}_{i=1}^J$ can be converted into explicit inexact gradient information via solving a linear inverse problem from straightforward Taylor approximation. We call this method EGI – Ensemble-based gradient inference. Section 3 develops EGI-CBO, a consensus-based optimization method augmented by inexact gradient information. Finally, Section 4 generalizes this idea to ensemble-based sampling methods which normally use exact gradient evaluation, but can be shown to work with inexact gradients supplied by EGI as well.

2 Ensemble-based gradient inference (EGI) from pointwise ensemble evaluation

Consider an unknown function $V : \mathbb{R}^d \rightarrow \mathbb{R}$ evaluated pointwise in an ensemble $\{x^k\}_{k=1}^J \subset \mathbb{R}^d$. Our goal is to infer gradient information (as well as possibly higher-order derivatives) at one or each of the ensemble members’ positions x^j , i.e. $\nabla V(x^j)$ (and possibly higher-order derivatives). In short, we want to solve the ill-posed problem

$$\{V(x^k)\}_{k=1}^J \mapsto \nabla V(x^*),$$

where x^* is an element of the ensemble $\{x^k\}_{k=1}^J$ ². We now describe our approach where we set $x^* = x^j$ for some fixed $j \in \{1, \dots, J\}$. By Taylor's formula, for any $i \in \{1, \dots, J\}$,

$$\begin{aligned} V(x^i) - V(x^j) &= \nabla V(x^j)^T (x^i - x^j) \\ &\quad + \frac{1}{2} (x^i - x^j)^T HV(x^j) (x^i - x^j) + \varepsilon_i^j \cdot \frac{\|x^i - x^j\|^3}{6}, \end{aligned}$$

where we model the action of the unknown tensors $D^3V(x^j)$ on $[x^i - x^j, x^i - x^j, x^i - x^j]$ by independent random variables $\{\varepsilon_i^j\}_{i=1}^J \sim N(0, \gamma^2)$. We make the ansatz $\nabla V(x^j) \approx \sum_{k=1}^J u_k^{j,1} \frac{x^k - x^j}{\|x^k - x^j\|}$ and $HV(x^j) \approx \sum_{k=1}^J u_k^{j,2} \frac{(x^k - x^j)}{\|x^k - x^j\|} \otimes \frac{(x^k - x^j)}{\|x^k - x^j\|}$ for $u_k^{j,1}, u_k^{j,2} \in \mathbb{R}$ yet to be determined. Clearly, this means that our approximation for ∇ will be an element of the affine space spanned by the ensemble, also HV is now approximated by a rank- J matrix. We introduce an additional error slack term $\xi > 0$, which will be used for localization purposes, see Remark 2.3. Then

$$\begin{aligned} V(x^i) - V(x^j) &= \sum_{k=1}^J u_k^{j,1} \cdot \frac{(x^k - x^j)^T (x^i - x^j)}{\|x^k - x^j\|} \\ &\quad + \frac{1}{2} \sum_{k=1}^J u_k^{j,2} \cdot \left[\frac{(x^k - x^j)^T (x^i - x^j)}{\|x^k - x^j\|} \right]^2 + \varepsilon_i^j \cdot \left(\frac{\|x^i - x^j\|^3}{6} + \xi \right). \end{aligned}$$

Remark 2.1. For consistency, we set $0/0 = 0$ here.

Remark 2.2. Alternatively we could include mixed terms in the formulation of $HV(x^j)$, i.e. $HV(x^i) \approx \sum_{k,l} u_{k,l}^{j,2} \frac{(x^k - x^j)}{\|x^k - x^j\|} \otimes \frac{(x^l - x^j)}{\|x^l - x^j\|}$ for $u_{k,l}^{j,2} \in \mathbb{R}$. Note that this comes at the cost that the number of coefficients scales with J^2 instead of J . For simplicity of presentation, we stick with the rank- J ansatz for $HV(x^j)$.

Remark 2.3. The motivation for the introduction of the error slack term ξ is two-fold: First, if there are two ensemble members x^i, x^j very close to each other, then this error term acts as a safeguard against unwanted overfitting. Second, if all ensemble members are very close to each other (in the magnitude of machine precision), then it buffers unwanted numerical instability. This error term can also be removed from the model by setting $\xi = 0$. On the other hand, letting $\xi \rightarrow \infty$ recovers the least-squares quadratic regression function through the data points, under the additional condition that the regression function passes through $(x^j, V(x^j))$. In a sense, $\xi = 0$ corresponds to “local” gradient information, because it takes into account mostly nearby points, and $\xi \rightarrow \infty$ yields “global” gradient information. The effect of ξ is illustrated in Figure 1.

We now describe how to set up gradient inference as a linear inverse problem.

2.1 Ensemble-based gradient inference as an inverse problem

Let $\{x^i\}_{i=1}^J$ be an ensemble of points with pointwise evaluations $\{V(x^i)\}_{i=1}^J$ of an unknown function V . We fix $j \in \{1, \dots, J\}$, and our goal is to infer $\nabla V(x^j)$ (and $HV(x^j)$) from the

²It is conceivable to allow x^* to be an arbitrary point “near” the ensemble by appropriately modifying the ansatz below.

data. We set the following notational shorthands:

$$\begin{aligned} X^j &= (x^1 - x^j, \dots, x^i - x^j, \dots, x^J - x^j) \in \mathbb{R}^{d \times J}, & X_{:,i}^j &= x^i - x^j, \\ Z^j &= \left(\frac{x^1 - x^j}{\|x^1 - x^j\|}, \dots, \frac{x^J - x^j}{\|x^J - x^j\|} \right) \in \mathbb{R}^{d \times J}, & Z_{:,i}^j &= \frac{x^i - x^j}{\|x^i - x^j\|}, \\ y^j &= (V(x^1) - V(x^j), \dots, V(x^J) - V(x^j))^T \in \mathbb{R}^J, & y_i^j &= V(x^i) - V(x^j). \end{aligned}$$

Then with $u^{j,i} = (u_k^{j,i})_{k=1}^J \in \mathbb{R}^J$ and $u^j = (u^{j,1}, u^{j,2}) \in \mathbb{R}^{2J}$,

$$y^j = \begin{bmatrix} X^{jT} Z^j & \frac{(X^{jT} Z^j)^{\odot 2}}{2} \end{bmatrix} \cdot \begin{pmatrix} u^{j,1} \\ u^{j,2} \end{pmatrix} + \left(\frac{1}{3!} \text{diag}(\{\|x^i - x^j\|^3\}_{i=1}^J) + \xi \right) \cdot \varepsilon^j, \quad (2.1)$$

where the Hadamard square $(X^{jT} Z^j)^{\odot 2}$ is taken component-wise, i.e. $[(X^{jT} Z^j)^{\odot 2}]_{i,j} = [(X^{jT} Z^j)_{i,j}]^2$. We can further compact this form by setting $A^j = (X^{jT} Z^j, \frac{(X^{jT} Z^j)^{\odot 2}}{2}) \in \mathbb{R}^{d \times (2J)}$ and $\Gamma_{\xi, \gamma}^j = \left(\frac{\gamma^2}{3!} \text{diag}(\{\|x^i - x^j\|^3\}_{i=1}^J) + \xi \gamma^2 \right)$. Then

$$y^j = A^j u^j + \varepsilon^j \quad (2.2)$$

with $\varepsilon^j \sim N(0, \Gamma_{\xi, \gamma}^j)$ is a linear inverse problem for the coefficient vector u^j . If \bar{u}^j is the least squares solution of this inverse problem, then we can recover gradient information via

$$G_{\xi}^j(\{x^i\}_{i=1}^J) := Z^j \cdot \bar{u}^{j,1} = \sum_{k=1}^J \bar{u}_k^{j,1} \frac{x^k - x^j}{\|x^k - x^j\|} \approx \nabla V(x^j) \quad (2.3)$$

$$H_{\xi}^j(\{x^i\}_{i=1}^J) := \sum_{k=1}^J \bar{u}_k^{j,2} \frac{x^k - x^j}{\|x^k - x^j\|} \otimes \frac{x^k - x^j}{\|x^k - x^j\|} \approx HV(x^j) \quad (2.4)$$

This notation hides the implicit dependence on V , and the specific way u^j is obtained (although we assume this to be the least square solution to (2.2) unless stated otherwise). For brevity we write $G^j(\{x^i\}_{i=1}^J) := G_0^j(\{x^i\}_{i=1}^J)$ in the case $\xi = 0$ and similar for the Hessian H^j . Details of the inference are given in Algorithm 1. In the following we will refer to the case $\xi = 0$ as *local approximation* and $\xi > 0$ *global gradient approximation*. This characterization is motivated by the observation that ξ enters the error term in (2.1). Therefore, for $\xi = 0$, the Taylor approximation in the location of a particle x^i close to x^j needs to be much better than in any particle far away from x^j . In the other extreme case $\xi \rightarrow \infty$ all particles enter with equal weight in the gradient approximation, hence the second-order polynomial approximation will be a ‘‘global’’ approximation instead of a local Taylor approximation. See Figure 1 for a visualization of the effect of ξ .

Remark 2.4. The Hessian approximation can be written compactly in Python Einstein sum notation via $H^j(\{x^i\}_{i=1}^J) = \text{np.einsum}('k, \text{lk}, \text{mk} \rightarrow \text{lm}', \bar{u}^{j,2}, Z^j, Z^j)$.

Algorithm 1: Ensemble-based Gradient Inference (EGI)

- Data:** $\{x^i, V^i\}_{i=1}^J, \gamma > 0, \xi \geq 0, j \in \mathbb{N}$
Result: $G = G_\xi^j(\{x^i\}_{i=1}^J), H = H_\xi^j(\{x^i\}_{i=1}^J)$ (approx. to $\nabla V(x^j)$ and $HV(x^j)$)
- 1 $X \leftarrow (x^1 - x^j, \dots, x^J - x^j) \in \mathbb{R}^{d \times J}$
 - 2 $Z \leftarrow \left(\frac{x^1 - x^j}{\|x^1 - x^j\|}, \dots, \frac{x^J - x^j}{\|x^J - x^j\|} \right) \in \mathbb{R}^{d \times J}$
 - 3 $y \leftarrow (V^1 - V^j, \dots, V^J - V^j) \in \mathbb{R}^J$
 - 4 $A \leftarrow (X^T Z, \frac{1}{2}(X^T Z) \odot 2) \in \mathbb{R}^{d \times (2J)}$
 - 5 $\Gamma \leftarrow \gamma^2 \cdot \left[\frac{1}{3!} \text{diag}(\|x^i - x^j\|^3)_{i=1}^J + \xi \right] \in \mathbb{R}^{d \times d}$
 - 6 $(u^1, u^2)^T \leftarrow \text{lsq}(\Gamma^{-1}A, \Gamma^{-1}y) // \text{Solve } \Gamma^{-1}A(u^1, u^2)^T = \Gamma^{-1}y \text{ via Least-Squares}$
 - 7 $G \leftarrow \sum_{k=1}^J u_k^1 \frac{x^k - x^j}{\|x^k - x^j\|}$
 - 8 $H \leftarrow \sum_{k=1}^J u_k^2 \frac{x^k - x^j}{\|x^k - x^j\|} \otimes \frac{x^k - x^j}{\|x^k - x^j\|}$
-

Remark 2.5. The least-squares approach can without major changes be turned into a Bayesian sampling algorithm for gradient and Hessian information by solving the linear inverse problem (2.2) via the Gaussian update formula, taking samples $\{u_n^j\}_n$, and propagating the samples u_n^j via a mapping similar to Equations (2.3) and (2.4). This is described in Algorithm 2, but we forgo fixing any notation for this in order to keep the presentation clearer. We just remark that any subsequent algorithm can be modified to use Bayesian samples of the approximated gradient (Algorithm 2) instead of the deterministic least squares approximation Algorithm 1, as will be done in Algorithm 8.

Algorithm 2: Bayesian Ensemble-based Gradient Inference

- Data:** $\{x^i, V^i\}_{i=1}^J, \gamma > 0, \xi \geq 0, \text{index } j \in \mathbb{N}, \Sigma > 0, \text{number of samples } N \in \mathbb{N}$
Result: samples $\{G^{n,j}\}_{n=1}^N, \{H^{n,j}\}_{n=1}^N$ (approximations to $\nabla V(x^j)$ and $HV(x^j)$) and Bayesian maximum-a-posteriori estimators $G_{\text{MAP}}, H_{\text{MAP}}$.
- 1 $X \leftarrow (x^1 - x^j, \dots, x^J - x^j) \in \mathbb{R}^{d \times J}$
 - 2 $Z \leftarrow \left(\frac{x^1 - x^j}{\|x^1 - x^j\|}, \dots, \frac{x^J - x^j}{\|x^J - x^j\|} \right) \in \mathbb{R}^{d \times J}$
 - 3 $y \leftarrow (V^1 - V^j, \dots, V^J - V^j) \in \mathbb{R}^J$
 - 4 $A \leftarrow (X^T Z, \frac{1}{2}(X^T Z) \odot 2) \in \mathbb{R}^{d \times (2J)}$
 - 5 $\Gamma \leftarrow \gamma^2 \cdot \left[\frac{1}{3!} \text{diag}(\|x^i - x^j\|^3)_{i=1}^J + \xi \right] \in \mathbb{R}^{d \times d}$
 - 6 $K \leftarrow \Sigma A^T (\Gamma + A \Sigma A^T)^{-1}$
 - 7 $\hat{\mu} \leftarrow (\hat{\mu}^1, \hat{\mu}^2) \leftarrow Ky$
 - 8 $\hat{\Sigma} \leftarrow \Sigma - K A \Sigma$
 - 9 $G_{\text{MAP}} \leftarrow \sum_{k=1}^J \hat{\mu}_k^1 \frac{x^k - x^j}{\|x^k - x^j\|}$
 - 10 $H_{\text{MAP}} \leftarrow \sum_{k=1}^J \hat{\mu}_k^2 \frac{x^k - x^j}{\|x^k - x^j\|} \otimes \frac{x^k - x^j}{\|x^k - x^j\|}$
 - 11 **for** $n \leftarrow 1$ **to** N **do**
 - 12 $(u^{1,n}, u^{2,n})^T \sim \mathcal{N}(\hat{\mu}, \hat{\Sigma}) // \text{sample from posterior}$
 - 13 $G^{n,j} \leftarrow \sum_{k=1}^J u_k^{1,n} \frac{x^k - x^j}{\|x^k - x^j\|}$
 - 14 $H^{n,j} \leftarrow \sum_{k=1}^J u_k^{2,n} \frac{x^k - x^j}{\|x^k - x^j\|} \otimes \frac{x^k - x^j}{\|x^k - x^j\|}$
-

Remark 2.6. The numerical complexity of Algorithms 1 and 2 is dominated by the cost of solving a linear equation of size $J \times J$, since we assume pointwise evaluation of $V(x^i)$ to be available initially.

2.2 Examples

We illustrate the proposed approximation of gradient and Hessian with the help of two well-known benchmarks for optimization.

Rastrigin function in 1d We set $V : \mathbb{R} \rightarrow \mathbb{R}$ with $V(x) = x^2 + 3 \cdot (1 - \cos(2\pi x))$, which is (a slightly differently scaled variant of) the Rastrigin function. Figure 1 demonstrates how we can locally approximate a function from given pointwise evaluations. Note in particular how ξ can be used as a parameter for the degree of (non-)locality of the gradient approximation: $\xi = 0$ corresponds to local Taylor approximation while the case $\xi \gg 1$ approaches a least-squares quadratic fit through all data points (albeit always going through the current reference point $(x^j, V(x^j))$). The figure on the bottom right also shows local quadratic approximation samples obtained by interpreting (2.2) as a Bayesian inverse problem (after defining a prior on the coefficients u^j), taking i.i.d. samples \hat{u}^j from the posterior. All local approximate functions are built as follows: Starting from a coefficient vector \bar{u}^j (i.e. either least squares solution to (2.2) obtained with Algorithm 1 or posterior samples from Algorithm 2) we construct a quadratic approximative map via

$$x \mapsto V(x^j) + \left\langle G_\xi^j(\{x^i\}_{i=1}^J), x - x^j \right\rangle + \frac{1}{2} \left\langle x - x^j, H_\xi^j(\{x^i\}_{i=1}^J) \cdot (x - x^j) \right\rangle,$$

and plot this quadratic function alongside the graph of V .

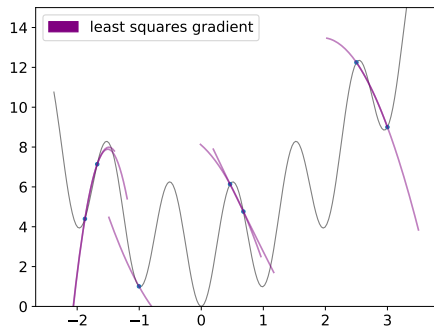
Himmelblau function in 2d As V we choose the Himmelblau function $V : (x, y) \mapsto (x^2 + y - 11)^2 + (x + y^2 - 7)^2$ on \mathbb{R}^2 and proceed along the same lines as for the Rastrigin function. Figure 2 shows the influence of J and ξ . The column on the right-hand side shows the level sets of

$$x \mapsto V(x^j) + (G_\xi^j(\{x^i\}_{i=1}^J))^T (x - x^j) + \frac{1}{2} (x - x^j)^T \cdot H_\xi^j(\{x^i\}_{i=1}^J) \cdot (x - x^j) \quad (2.5)$$

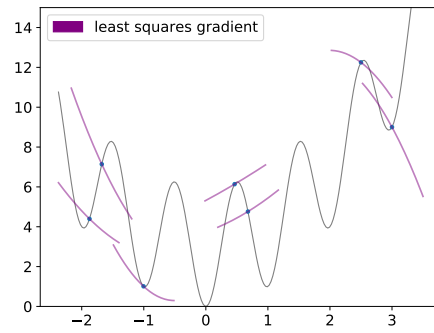
for an arbitrarily chosen “reference particle” x^j .

The left column of Figure 2 shows (for an ensemble $(x^j, V(x^j))_j$) a comparison between true gradients $\nabla V(x^j)$ and the least squares approximations obtained from Algorithm 1. Note that the arrows are scaled to the same magnitude, so only the angle between ground truth and inferred gradient is a relevant measure of approximation quality. Note that taking a larger ensemble improves the local gradient approximation, as to be expected. The right column shows level sets of the quadratic function in Equation (2.5). For $\xi = 0$, the quadratic approximation to V obtained from (inferred) gradient and Hessian works well only locally, while the global approximation $\xi = 1000$ shows deficits when judging actual gradient approximation (as can be seen by comparing the arrows in the figures belonging to $J = 25, \xi = 0$ with $J = 25, \xi = 1000$). This is a similar phenomenon as shown in Figure 1. Finally, Figure 3 shows an illustration of Algorithm 2. It shows how the true gradient $\nabla V(x^i)$ in a specific ensemble member x^i is approximated. In the smaller ensemble of size $J = 5$, the posterior gradient samples predominantly point along a direction different to the true gradient, but the latter can be seen to be in the support of this measure. By increasing the ensemble size to $J = 25$ and thereby providing more information, it can be seen that the support of the posterior measure aligns with and contracts on the true gradient.

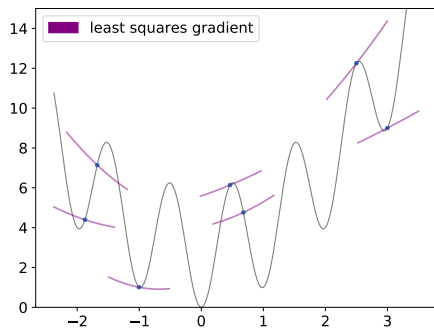
We now describe a series of examples of optimization and sampling algorithms which can be augmented with the gradient approximation presented above.



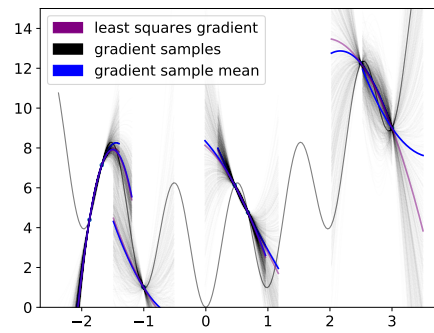
(a) Least squares solutions, $\xi = 0$



(b) Least squares solutions, $\xi = 1$

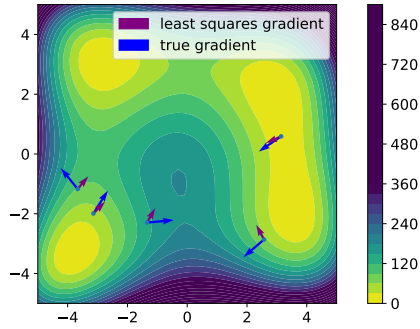


(c) Least squares solutions, $\xi = 1000$

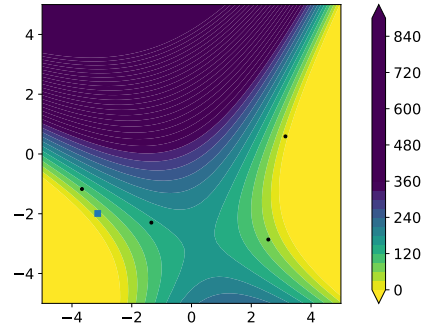


(d) $\xi = 0$ and quadratic approximations obtained from samples from posterior distribution on coefficients u^j .

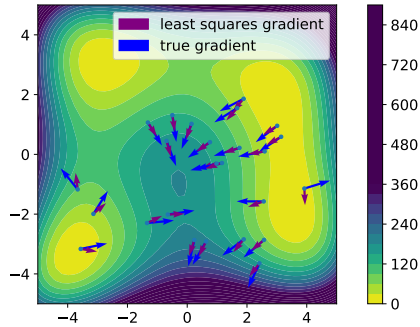
Figure 1: Approximation of (a variant of) the Rastrigin function $x \mapsto x^2 + 3(1 - \cos(2\pi x))$ via finite evaluations with various choices of ξ . Code: `1d_gradinf.py`



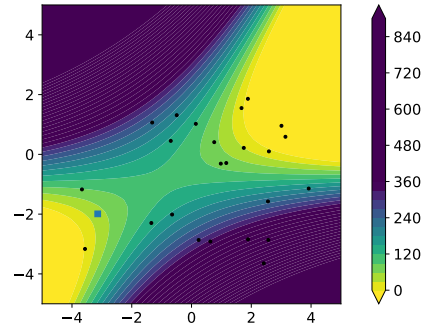
(a) $J = 5, \xi = 0$



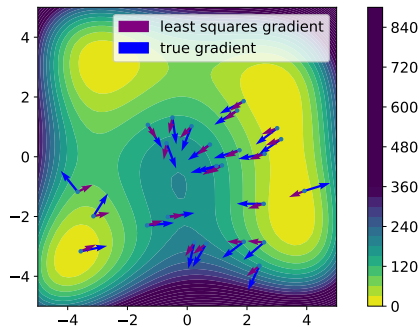
(b) quadratic approximation centered at x^j (marked with square).



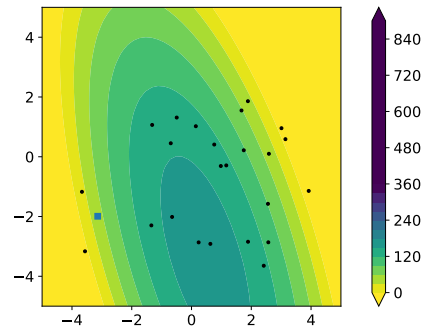
(c) $J = 25, \xi = 0$



(d) quadratic approximation centered at x^j (marked with square).



(e) $J = 25, \xi = 1000$



(f) quadratic approximation centered at x^j (marked with square).

Figure 2: Approximation of Himmelblau function by pointwise evaluation. Left column shows approximated gradients $G^j(\{x^i\}, V)$ in comparison to actual gradients (vectors are rescaled to unit length). Right columns show quadratic function obtained by extending local quadratic inferred approximation to whole domain. Code: `2d_gradinf_J5_xi0.py`, `2d_gradinf_J25_xi0.py`, `2d_gradinf_J25_xi1000.py`

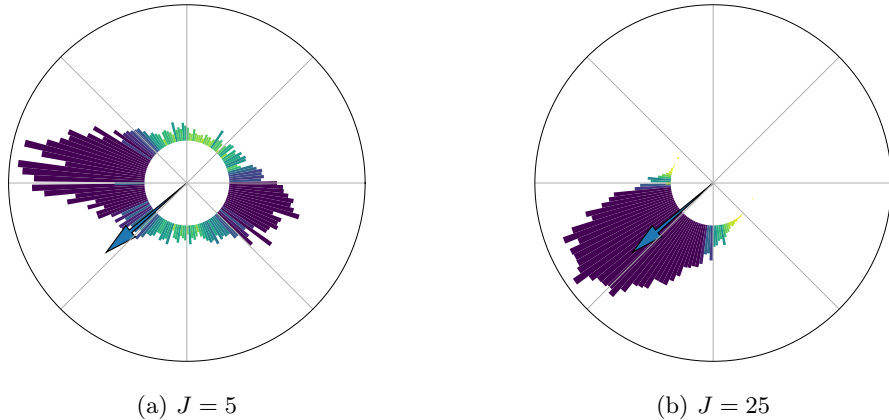


Figure 3: Posterior gradient samples after choosing a prior on the coefficients u^j : Radial histogram of gradient (direction) samples, evaluated at a specific ensemble member, with true gradient (blue arrow) for reference. Clearly, increasing the number of ensemble members J contracts the Bayesian posterior around the ground truth gradient vector. Note that magnitude of any gradient vectors is disregarded in this illustration. Code: `2d_bayes_gradinf.py`

3 Consensus-based optimization augmented by EGI

For optimization problems with unknown structure it is advantageous to have gradient-free optimization algorithms that allow for treating the objective as black-box. Therefore the original formulation of CBO does not use any gradient information. With the gradient inference idea discussed above, we are able to keep the gradient-free property of CBO and still augment the algorithm with higher order differential information.

3.1 EGI-CBO

Let $V : \mathbb{R}^d \rightarrow [0, \infty)$ be a (possibly non-convex) function, $\beta > 0$ an inverse heat parameter. We propose the following gradient-EGI-CBO method describing the dynamics of the particles via

$$dx^i = -\kappa G_{\xi}^0(\{\mathbf{m}_{\beta}(\rho), x^1, \dots, x^J\}) dt - \lambda(x^i - \mathbf{m}_{\beta}) dt + \sigma|x^i - \mathbf{m}_{\beta}| dW_t^i \quad (3.1)$$

with initial conditions $x_0^i \sim \mathcal{P}_2(\mathbb{R}^d)$ drawn independently. Note that the ensemble is augmented by the weighted mean and we take the least square gradient and Hessian approximation centered at the weighted mean and use this gradient approximation for all particles. The full algorithm for this method – EGI-CBO – can be found in Algorithm 3.

The difference to CBO is the additional (approximated) gradient term. The motivation for incorporating this is threefold: (1) Assuming that the spatial resolution of the ensemble is coarser than the distance of individual minima and the ensemble is still spread out, the gradient term can help to jump over local minima. (2) The gradient term converges to the true gradient projected onto the affine subspace spanned by the ensemble. This may facilitate the convergence to the true global minimizer. Indeed, by the Laplace principle and the quantitative non-asymptotic Laplace principle Fornasier et al. (2021b) the approximation quality of CBO strongly depends on the temperature parameter. Additional gradient

information is expected to improve the approximation quality, and drive the weighted mean towards the true minimizer. (3) In the later phase of the dynamics, the additional gradient term helps with accelerated collapse around the actual position of the (possibly local) minimum. This alleviates an issue of CBO where the ensemble does indeed collapse in a vicinity of a (possibly local) minimum x^* , but with consensus not necessarily converging to the actual position of x^* . Both features, “convergence to better minima” and “better convergence to minima”, can be seen from the following numerical experiments.

3.2 Numerical examples: EGI-CBO

For simplicity, we use the least squares version (Algorithm 1) for the gradient approximation for the following results. Note that a sampling approach via Algorithm 2 is feasible as well and might be preferred in Machine Learning applications as the behaviour resembles stochastic gradient descent methods.

Algorithm 3: EGI-CBO

Data: $N \in \mathbb{N}$, $\{x_0^j\}_{j=1}^J$, $\alpha, \lambda, \sigma, \kappa, \xi, \tau \geq 0$,
noise $\in \{\text{norm-proportional, component-wise}\}$
Result: minimizer m_β of I

```

1 for  $n \leftarrow 0$  to  $N - 1$  do
2    $m_n^\alpha \leftarrow \frac{\sum_{j=1}^J \exp(-\alpha I(x_n^j)) \cdot x_n^j}{\sum_{j=1}^J \exp(-\alpha I(x_n^j))}$  // Weighted mean - use logsumexp to avoid underflow
3    $m_n \leftarrow \frac{1}{J} \sum_{j=1}^J x_n^j$  // Unweighted mean
4   for  $j \leftarrow 1$  to  $J$  do
5      $g_n \leftarrow G^0(\{m_n\} \cup \{x_n^i\}_{i=1}^J, I)$  // Gradient approximation (least squares) at
      unweighted mean, via Algorithm 1
6      $W_n^j \sim N(0, I^d)$ 
7     switch noise do
8       case norm-proportional do
9          $\sigma_n^j \leftarrow \sigma \|x_n^j - m_n^\alpha\| W_n^j$ 
10      case component-wise do
11         $\sigma_n^j \leftarrow \sigma (x_n^j - m_n^\alpha) \odot W_n^j$ 
12    $x_{n+1}^j \leftarrow x_n^j - \tau \kappa g_n - \tau \lambda (x_n^j - m_n^\alpha) + \sqrt{\tau} \sigma_n^j$  // Euler-Maruyama step

```

Remark 3.1. If we choose $\lambda = 0$ and $\sigma = 0$ in Algorithm 3, then this corresponds to a kind of ensemble-based gradient descent method. Unfortunately this seems to perform quite badly in practice: When the ensemble moves to a position such that its least squares approximation has a vanishing gradient (and this happened frequently in our numerical experiments), then the iteration essentially stops, without approaching the minimizer any further. For example, imagine $V(x) = x^2$, and ensemble of size $J = 2$ at positions -1 and $+1$. Then the estimated gradient will be 0, i.e. the ensemble will not move any further (although this issue can be alleviated by extrapolating gradients via second-order differential information, as done in Algorithm 7). The impact of contraction and stochastic exploration means that this cannot happen easily with EGI-CBO.

Rastrigin function in 2d We aim to minimize the two-dimensional Rastrigin function $V(x_1, x_2) = 2 \cdot 10 + x_1^2 - 10 \cos(2\pi x_1) + y_1^2 - 10 \cos(2\pi y_1)$. We start with an ensemble of $J = 4$ particles, which is a moderately large ensemble in two dimensions, and we also consider the

case of $J = 2$, which yields an ensemble spanning an affine subspace of dimension 1 in each iteration. We further set $\alpha = 100$, $\lambda = 1.5$, $\sigma = 0.7$, $\kappa = 0.5$, $\xi = 0$, $\tau = 0.01$ and $N = 1000$ iterations. Note that we choose the initial ensemble uniform in the set $[-4, -1]^2$, which does not contain the global minimum. As discussed in Kalise et al. (2022), this is a much harder case where only few studies of the CBO method exist.

The results can be observed in Figure 4: Here we compare CBO and EGI-CBO with ensemble sizes $J = 4$ and $J = 2$. We run 100 Monte Carlo simulations (with the same initial ensemble but independently sampled noise in the iterations) for each of these four settings and plot the position of the final iteration’s weighted mean as a black dot in the function domain. We also superimpose a 2d histogram to give a sense of the distribution of final weighted means of the MC simulations. We can make out the following features:

- Convergence towards local minima: It can be observed that the CBO dynamics tends to terminate in a local minimum (and never in the global minimum), but on a position with nonvanishing slope of f . This is due to the fact that the weighted mean acts as a barrier to the left of the ensemble: The particle closest to the weighted mean experience little to none drift or diffusion itself, with approaching particles being attracted to it. This is resolved by the approximate gradient term in EGI-CBO.
- Exploration of “better minima”. Due to the gradient term in EGI-CBO, the ensemble is able to experience a substantial shift along the essential slope of f , even surpassing some intermittent local minima. CBO on the other hand can only exhibit deterministic contraction towards \mathfrak{m}_β and stochastic exploration (which ignores the shape of f). Note that this effect is stronger for “global” EGI-CBO with $\xi > 0$, see below.
- This holds to some extent also in the underdetermined case $J = 2$, although convergence towards local minima is only slightly accelerated: With only two live particles, gradient information will never point directly towards local minimum.

Remark 3.2. In addition to the observations discussed above, the EGI-CBO turns out to reliably find various local minima of the highly multi-modal function within 100 Monte Carlo runs. This opens a new field of applications for CBO and might be worth to be investigated in future work.

Himmelblau function in 2d In contrast to the Rastrigin function with steep valleys the Himmelblau function is rather flat in the neighborhood of its minima. We also compare the behaviour of CBO and EGI-CBO in this setting. The Himmelblau function exhibits four global minima with value 0. Figure 5 shows a comparison of a single run of CBO with 64 particles and a single run of EGI-CBO with only 3 particles. We remark that all our experiments show similar results, so we show only one specific instance. This allows us to better represent the dynamics. It can be observed that EGI-CBO actually converges to one of the global minima, with an exponential rate, while the ensemble of CBO collapses to a point close to a minimum, but not towards the minimum itself. The function value of \mathfrak{m}_β decreases in discrete jumps. This corresponds to ensemble members crossing “better level sets” which influences \mathfrak{m}_β . EGI-CBO on the other hand strongly profits from a continuous drift towards a minimum.

High-dimensional smooth example To further highlight the advantages of the gradient augmentation, we employ a high-dimensional smooth convex example, $V : x \mapsto \frac{1}{2}\|x -$

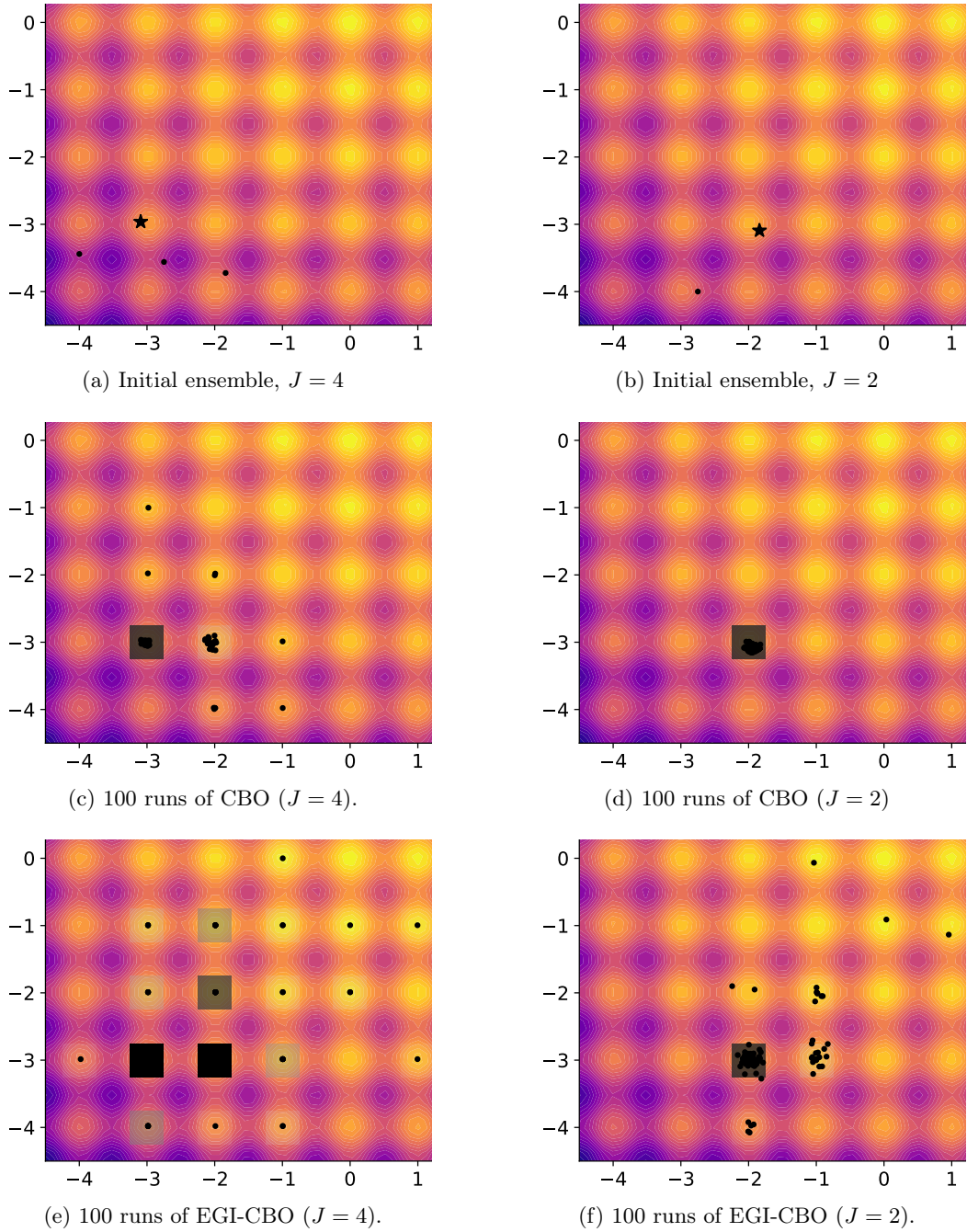
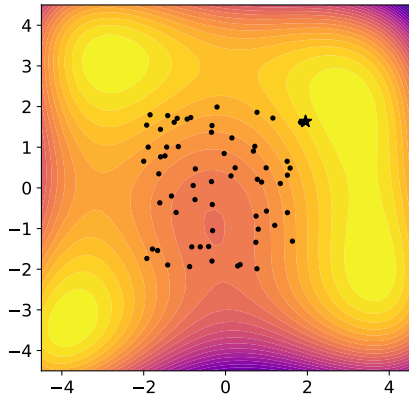
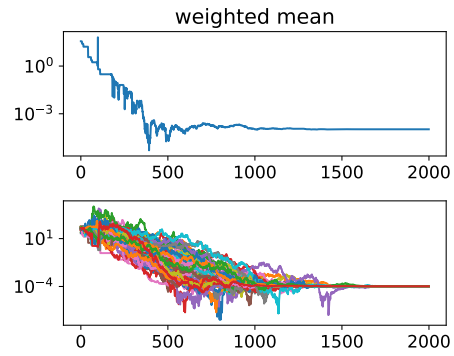


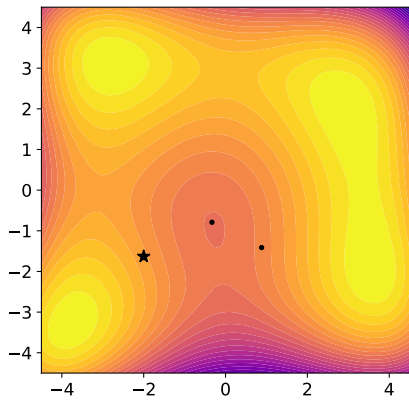
Figure 4: Code: `testMC_cbo_2d_rastrigin.py`, `testMC_cbo_2d_rastrigin_J2.py`, `testMC_aug_cbo_2d_rastrigin.py`, `testMC_aug_cbo_2d_rastrigin_J2.py`



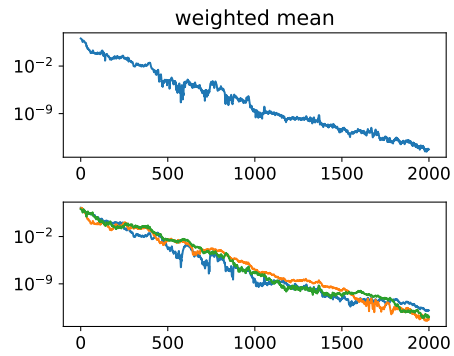
(a) Initial ensemble $J = 64$ (black dots) with initial weighted mean (star)



(b) One representative run of CBO ($J = 64$).



(c) Initial ensemble $J = 3$ (black dots) with initial weighted mean (star)



(d) One representative run of EGI-CBO ($J = 3$).

Figure 5: Application of CBO and EGI-CBO to the Himmelblau test function. Code: `test_cbo_2d_himmelblau.py`, `test_aug_cbo_2d_himmelblau.py`

$(1, \dots, 1)\|^2$ on \mathbb{R}^d , where $d = 10$. Clearly, $x = (1, \dots, 1)$ is the global minimum of V . We sample the initial ensemble uniformly on $[-4, -1]^d$ and emphasize that this domain excludes the global minimum. For the parameters, we set $\alpha = 100$, $\lambda = 1$, $\sigma = 0.2$ and we use component-wise noise for dimension-robustness. We start with the over-determined case $J = 20$. EGI-CBO ($\kappa = 4.0$) exhibits exponential convergence, which is not that surprising given that it essentially performs gradient descent, with its ensemble size having enough descriptive power to span the full space. Vanilla CBO does not converge to the minimum due to contraction of the ensemble on a point different from the minimum. The fact that the initial ensemble is far away from the minimum is an additional adversarial factor. Further experiments show that this is not resolved by increasing the noise term as the stochastic dynamics becomes unstable for a noise level larger than a certain threshold, even for component-wise noise.

Remark 3.3. We want to emphasize that this is not in contradiction with the theory for CBO Carrillo et al. (2018); Fornasier et al. (2021b) as the proofs consider the mean-field setting where the diffusion instantaneously extends the support of the distribution to the whole domain, and many proofs assume additionally that the unique global minimizer is contained in the support of the initial distribution.

The case $J = 5$ is more interesting: While CBO performs badly (as to be expected, see Remark 3.3), EGI-CBO is subjected to enough noise that accumulated gradient information brings this underdetermined ensemble quite close to the global minimum, although the ensemble has size lower than the spatial dimension.

In the previous numerical examples the additional smoothing error term in (2.1) is switched off ($\xi = 0$). As discussed in Figure 1 this corresponds to local gradient approximations. In next section we study the influence of nonlocal gradient approximations.

3.3 Global versus Local EGI-CBO

Figure 1 showing global EGI for the one-dimensional Rastrigin function suggests that “global” EGI-CBO (i.e. $\xi > 0$) can lead to improved exploration behaviour. In the following we investigate the influence of ξ in more detail. We therefore employ EGI-CBO as described in algorithm 3 with $\xi > 0$. This means that line 4 is modified to $g_n \leftarrow G_\xi^0(\{m_n\} \cup \{x_n^i\}_{i=1}^J)$ (i.e. with explicit dependence on ξ), where we now compare the settings $\xi = 0$ and $\xi > 0$ for varying values. We set $\lambda = 1.0$, $\sigma = 0.5$ and in the augmented case we have additionally $\kappa = 2.0$ as well as $\xi = 100$. Parameters of the time discretization are $T = 10$, $\tau = 0.01$. In Figure 7 we note that augmentation drives the ensemble towards the true minimizer. In contrast, the reference solution of CBO gets stuck in higher level set regions.

3.4 Discussion of EGI-CBO

To conclude the section on EGI-CBO we discuss some limitations of the method.

Subexponential convergence to higher-order minima. For further investigation of the speed of convergence, we choose $V(x) = \|x\|^4$ in $d = 50$ and set $J = 10$, $\kappa = 2.5$, $\sigma = 0.2$, $\lambda = 2.5$. In contrast to $\|x - (1, \dots, 1)\|^2$, where EGI-CBO performed very nicely, we note that the gradient of V vanishes rapidly in the neighborhood of the global minimum vanishes. Figure 8 indicates that flat regions around the minimizer slightly diminish the advantage of EGI-CBO over vanilla CBO. Indeed, EGI-CBO exhibits only subexponential convergence.

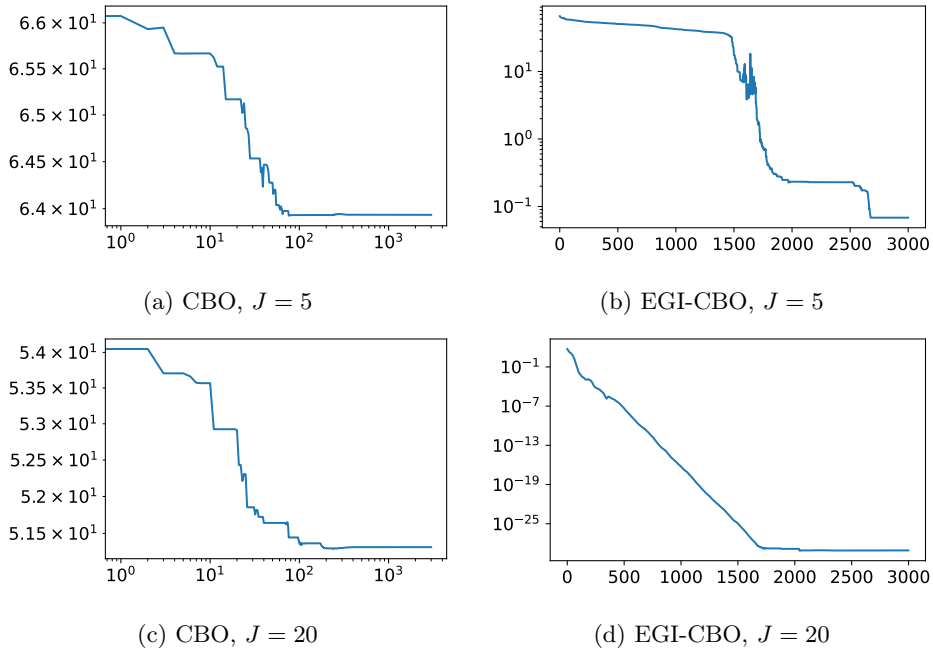
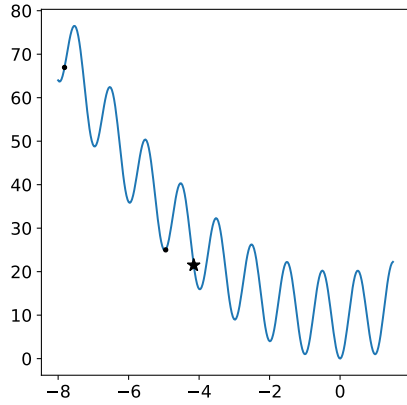
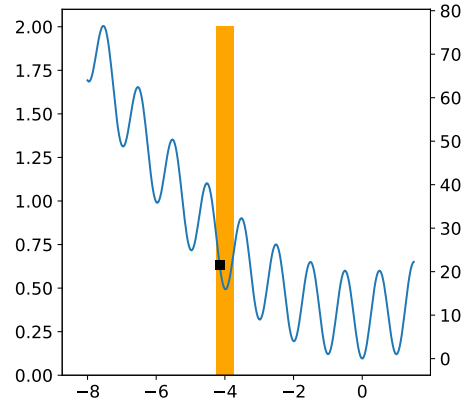


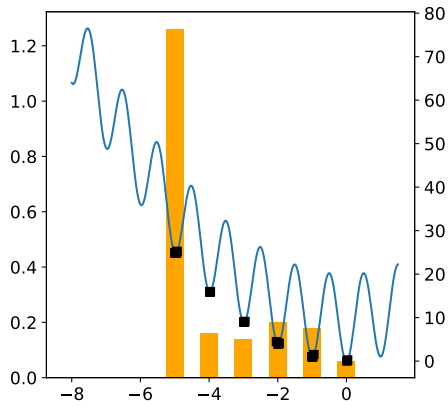
Figure 6: Performance of CBO and EGI-CBO on the function $V : x \mapsto \|x - (1, \dots, 1)\|^2$ in \mathbb{R}^{10} . Diagrams show evaluation of V on the weighted mean over the course of the whole iteration. Note that CBO is plotted over log-iterations in contrast to EGI-CBO, which is plotted over linear iterations. CBO levels off close to the initialization, with exponentially growing plateau lengths, while EGI-CBO converges exponentially fast to the global minimum (more quickly for larger ensembles, with jumps for smaller ensembles). Code: `test_cbo_ndnorm.py`



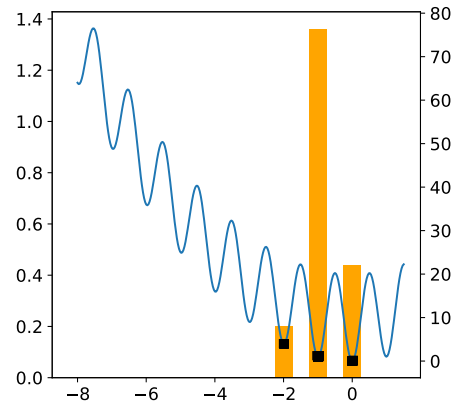
(a) Initial ensemble ($J = 3$) chosen for all simulations. Star marks weighted mean.



(b) Histogram of final weighted mean of 100 runs of CBO. All results are equal to the initial weighted mean of the ensemble.



(c) Histogram of final weighted mean of 100 runs of EGI-CBO ($\xi = 0$).



(d) Histogram of final weighted mean of 100 runs of global EGI-CBO ($\xi > 0$).

Figure 7: Demonstration of benefits of global EGI-CBO for multimodal optimization. Code: `testMC_cbo_globalapprox_1d_rastrigin.py`

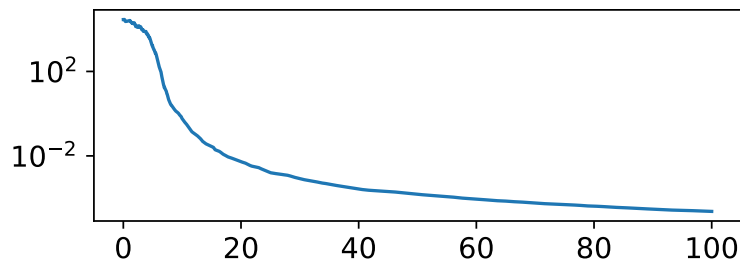


Figure 8: Convergence toward a higher-order minimum.

Nevertheless, it still outperforms CBO which does not converge to the minimum at all. (The latter fact is not demonstrated here, but experiments show the same behaviour as for the test function $\|x - (1, \dots, 1)\|^2$ above).

Very high-dimensional multimodal functions. In the literature Carrillo et al. (2021); Pinnau et al. (2017) very good performance of CBO for the high-dimensional ($d = 20$) Rastrigin function is reported. In order to achieve this performance, it is necessary to either set $J \gg d$ Pinnau et al. (2017) or $\sigma \gg \lambda$ Carrillo et al. (2021). In the latter case the diffusion dominates the drift towards the weighted mean, thus leaving the contractive domain of CBO which was established in the theory (Carrillo et al., 2021, Theorem 3.2). In particular, CBO exhibits a random exploration with a slight bias towards the weighted mean, and contraction of the ensemble does not happen. Employing additional gradient information in this non-contractive domain of CBO, leads to numerical instabilities which do not improve the performance of vanilla CBO.

Smooth unimodal objective functions. If V is a smooth unimodal function with convex (or “nearly convex”) structure – for example the typical inverse elliptical problem for strongly informative data – CBO should not be used, as other methods typically have much better performance. Similarly, if true gradient is cheap to obtain, CBO is probably not the method of choice as it requires many function evaluations. Nevertheless, for real-world applications often no structure is known a-priori and only functions evaluations are available. Then (augmented) CBO is a competitive alternative to other population based methods, which is furthermore backed-up by theoretical convergence proofs.

4 Gradient-based sampling using EGI

In contrast to our approach with CBO (a completely gradient-agnostic method which we augmented via inexact gradients), we now describe how some gradient-based sampling methods can be adapted to inexact ensemble-based gradients.

4.1 EGI-LS and EGI-MALA

We begin with the unconditioned case, i.e. $M = \text{Id}$ and propose the following gradient-free sampling method as substitute dynamics:

$$dx_t^j = -G^j(\{x^i\}_{i=1}^J) dt + \sqrt{2} dW_t^j \quad (4.1)$$

with initial condition $x_0^i \sim \mathcal{P}_2(\mathbb{R}^d)$ independently drawn for $i = 1, \dots, J$. A pseudocode for the implementation of the dynamics is given in Algorithm 4.

In the same spirit, we provide results for the other ensemble-based sampling algorithms presented in the introduction (see Section 1.1). Note that we set $\xi = 0$ by default. We expect that global gradient approximations lead to similar behaviour as in the optimization case. For some sampling applications it might make sense to allow for “global gradient approximations” (i.e. $\xi > 0$). For the sake of legibility we leave a detailed study to future investigations.

An Metropolis adjustment, the so-called MALA sampler, was proposed to improve the sampling accuracy of discretized Langevin dynamics in Roberts and Tweedie (1996). In our setting this yields a straight-foward generalization of MALA, the EGI-augmented

Metropolis-adjusted Langevin algorithm (EGI-MALA), see Algorithm 5.

Algorithm 4: EGI-augmented Langevin Sampler (**EGI-LS**)

Data: $N \in \mathbb{N}$, $\{x_0^j\}_{j=1}^J$, step size h
Result: samples $\{x_n^j\}_{j=1, n=1}^{J, N}$ from $d\mu/dx \propto \exp(-V(x))$

```

1 for  $n \leftarrow 0$  to  $N - 1$  do
2   for  $j \leftarrow 1$  to  $J$  do
3      $g_n^j = G^j(\{x_n^i\}_{i=1}^J)$  // approximate gradient in proposals, via Algorithm 1
4      $W_n^j \sim N(0, 1)$ ;
5      $x_{n+1}^j \leftarrow x_n^j - hg_n^j + \sqrt{2h}W_n^j$ ;
```

Algorithm 5: (EGI-MALA)

Data: $N \in \mathbb{N}$, $\{x_0^j\}_{j=1}^J$, $\tau > 0$
Result: samples $\{x_n^j\}_{j=1, n=1}^{J, N}$ from $d\mu/dx \propto \exp(-V(x))$

```

1 for  $n \leftarrow 0$  to  $N - 1$  do
2   for  $j \leftarrow 1$  to  $J$  do
3     if  $n \geq 1$  then
4        $g_n^j = G^j(\{x_n^i\}_{i=1}^J \cup \{\mu_{n-1}^i\}_{i=1}^J)$  // approximate gradient, via Algorithm 1
5     else
6        $g_n^j = G^j(\{x_n^i\}_{i=1}^J)$  // approximate gradient, via Algorithm 1
7      $W_n^j \sim N(0, I^d)$ 
8      $\text{prop}_n^j \leftarrow x_n^j - \tau g_n^j + \sqrt{2\tau}W_n^j$  // Langevin-type proposal
9      $\gamma_n^j = G^j(\{\text{prop}_n^i\}_{i=1}^J)$  // approximate gradient in proposals, via Algorithm 1
10    for  $j \leftarrow 1$  to  $J$  do
11       $q_{\text{fwd}}^j \leftarrow \exp(-\frac{1}{4\tau}\|\text{prop}_n^j - (x_n^j - \tau g_n^j)\|^2)$  // Metropolis adjustment
12       $q_{\text{bwd}}^j \leftarrow \exp(-\frac{1}{4\tau}\|x_n^j - (\text{prop}_n^j - \tau \gamma_n^j)\|^2)$ 
13       $\alpha_j \leftarrow \frac{\exp(-V(\text{prop}_n^j)) \cdot q_{\text{bwd}}^j}{\exp(-V(x_n^j)) \cdot q_{\text{fwd}}^j}$ 
14       $\xi \sim \text{Unif}[0, 1]$ 
15      if  $\xi \leq \alpha_j$  then
16         $x_{n+1}^j \leftarrow \text{prop}_n^j$ 
17         $\mu_n^j \leftarrow x_n^j$  // keep previous iterate as memory
18      else
19         $x_{n+1}^j \leftarrow x_n^j$ 
20         $\mu_n^j \leftarrow \text{prop}_n^j$  // Keep (rejected) proposal as memory
```

4.2 EGI-ALDI and EGI-EKS

The extraordinary feature of gradient-free ALDI is that it implicitly constructs and uses gradient information of V without the need of solving a linear system as demonstrated in 1.1. Unfortunately, this approximation fails if A is nonlinear.

For this reason, we also consider a new version of this methodology by replacing gradient-free ALDI's implicit gradient (biased for nonlinear forward maps) by our inexact gradient approximation via EGI, leading to the following sampling algorithm, EGI-ALDI (gradient-

free ALDI with estimated gradients):

Algorithm 6: gradient-free ALDI with estimated gradients (**EGI-ALDI**)

Data: $N \in \mathbb{N}, \{x_0^j\}_{j=1}^J, \tau > 0$
Result: samples $\{x_n^j\}_{j=1, n=1}^{J, N}$ from $d\mu/dx \propto \exp(-V(x))$

- 1 **for** $n \leftarrow 0$ **to** $N - 1$ **do**
- 2 $\bar{x}_n \leftarrow \frac{1}{J} \sum_{i=1}^J x_n^i$
- 3 $C_n^{1/2} \leftarrow \frac{1}{\sqrt{J}} (x_n^1 - \bar{x}_n, \dots, x_n^J - \bar{x}_n) \in \mathbb{R}^{d \times J}$
- 4 $C_n \leftarrow \frac{1}{J} \sum_{i=1}^J (x_n^i - \bar{x}) \otimes (x_n^i - \bar{x})$
- 5 **for** $j \leftarrow 1$ **to** J **do**
- 6 $g_n^j \leftarrow G^j(\{x_n^i\}_{i=1}^J \cup \{\bar{x}_n\})$ // approximate gradient in each particle (not in mean), via Algorithm 1
- 7 $W_n^j \sim N(0, I^J)$
- 8 $x_{n+1}^j \leftarrow x_n^j - \tau C_n \cdot g_n^j + \tau \frac{d+1}{J} (x_n^j - \bar{x}_n) + \sqrt{2\tau} C_n^{1/2} W_n^j$ // ALDI step

4.3 Gradient extrapolation

All methods presented so far employ gradient approximations computed in each ensemble point, see e.g. the **for**-loop in algorithm 2–5, which means that each iteration requires the solution of J linear equations (by evaluating $G^j(\{x_n^i\}_i, I)$ for $j = \{1, \dots, J\}$). It is possible to strongly cut down on computational complexity at the cost of introducing an additional source of error: Instead of approximating each gradient, we can approximate the gradient and Hessian only in a suitably chosen reference point x^* (e.g. the ensemble mean) and extrapolate:

$$\nabla V(x_n^j) \approx G^0(\{x^*\} \cup \{x_n^i\}_{i=1}^J) + H^0(\{x^*\} \cup \{x_n^i\}_{i=1}^J) \cdot (x_n^j - x^*), \quad (4.2)$$

which is reminiscent of $\nabla V(y) = \nabla V(x) + HV(x) \cdot (y - x) + o(\|y - x\|)$. Of course, this approximation is only valid if either the ensemble is sufficiently strongly concentrated or the measure is sufficiently Gaussian-like. To be more precise, we describe this variant for the EGI-ALDI algorithm:

Algorithm 7: gradient-free ALDI with estimated and **extrapolated** gradients (EGI-ALDI-extra)

Data: $N \in \mathbb{N}, \{x_0^j\}_{j=1}^J, \tau > 0$
Result: samples $\{x_n^j\}_{j=1, n=1}^{J, N}$ from $d\mu/dx \propto \exp(-V(x))$

- 1 **for** $n \leftarrow 0$ **to** $N - 1$ **do**
- 2 $\bar{x}_n \leftarrow \frac{1}{J} \sum_{i=1}^J x_n^i$
- 3 $C_n^{1/2} \leftarrow \frac{1}{\sqrt{J}} (x_n^1 - \bar{x}_n, \dots, x_n^J - \bar{x}_n) \in \mathbb{R}^{d \times J}$
- 4 $C_n \leftarrow \frac{1}{J} \sum_{i=1}^J (x_n^i - \bar{x}) \otimes (x_n^i - \bar{x})$
- 5 $g_n \leftarrow G^0(\{\bar{x}_n\} \cup \{x_n^i\}_{i=1}^J)$ // approximate gradient only in mean, via Algorithm 1
- 6 $H_n \leftarrow H^0(\{\bar{x}_n\} \cup \{x_n^i\}_{i=1}^J)$ // Hessian approximation in mean, via Algorithm 1
- 7 **for** $j \leftarrow 1$ **to** J **do**
- 8 $g_n^j \leftarrow g_n + H_n(x_n^j - \bar{x}_n)$
- 9 $W_n^j \sim N(0, I^J)$ // extrapolate estimated gradient
- 10 $x_{n+1}^j \leftarrow x_n^j - \tau C_n \cdot g_n^j + \tau \frac{d+1}{J} (x_n^j - \bar{x}_n) + \sqrt{2\tau} C_n^{1/2} W_n^j$ // ALDI step

By taking EGI-ALDI-extra and using a sampled gradient approximation (Algorithm 2) instead of the least square solution (Algorithm 1) we obtain Algorithm 8, although honestly mainly conceived for the sake of its acronym.

Algorithm 8: gradient-free ALDI with Bayesian Gradients (ALDI-BaG)

Data: $N \in \mathbb{N}$, $\{x_0^j\}_{j=1}^J$, $\tau > 0$
Result: samples $\{x_n^j\}_{j=1, n=1}^{J, N}$ from $d\mu/dx \propto \exp(-V(x))$

```

1 for  $n \leftarrow 0$  to  $N - 1$  do
2    $\bar{x}_n \leftarrow \frac{1}{J} \sum_{i=1}^J x_n^i$ 
3    $C_n^{1/2} \leftarrow \frac{1}{\sqrt{J}} (x_n^1 - \bar{x}_n, \dots, x_n^J - \bar{x}_n) \in \mathbb{R}^{d \times J}$ 
4    $C_n \leftarrow \frac{1}{J} \sum_{i=1}^J (x_n^i - \bar{x}) \otimes (x_n^i - \bar{x})$ 
5    $g_n \leftarrow G^0(\{\bar{x}_n\} \cup \{x_n^i\}_{i=1}^J)$  // approximate gradient only in mean, via Algorithm 2
6    $H_n \leftarrow H^0(\{\bar{x}_n\} \cup \{x_n^i\}_{i=1}^J)$  // Hessian approximation in mean, via Algorithm 2
7   for  $j \leftarrow 1$  to  $J$  do
8      $g_n^j \leftarrow g_n + H_n(x_n^j - \bar{x}_n)$  // extrapolate estimated gradient
9      $W_n^j \sim N(0, I^J)$ 
10     $x_{n+1}^j \leftarrow x_n^j - \tau C_n \cdot g_n^j + \tau \frac{d+1}{J} (x_n^j - \bar{x}_n) + \sqrt{2\tau} C_n^{1/2} W_n^j$  // ALDI step

```

4.4 Numerical example: Sampling from a two-dimensional non-Gaussian measure

We consider the inverse problem

$$y = A(x) + \varepsilon$$

with $A : \mathbb{R}^2 \rightarrow \mathbb{R}$, $A(x) = (x_2 - 2)^2 - (x_1 - 3.5) - 1$, $y = 0$, and $\varepsilon \sim N(0, \frac{1}{22})$. We set a Gaussian prior $\mu_0 = N(0_2, \tau^2 \cdot I)$ with $\tau = 2$ on the unknown parameter $x \in \mathbb{R}^2$. We write $\Phi(x) = \frac{1}{2\sigma^2} |y - A(x)|^2$, $I(x) = \Phi(x) + \frac{1}{2\tau^2} \|x\|^2$. This leads to a Bayesian posterior on the parameter μ^y of form

$$\frac{d\mu^y}{d\mu_0}(x) \propto \exp(-\Phi(x))$$

or

$$\frac{d\mu^y}{dx}(x) \propto \exp(-I(x)).$$

Figure 9 shows the result of applying various samplers. We compare Ensemble Langevin (EGI-LS), Ensemble MALA (EGI-MALA), gradient-free ALDI (Garbuno-Inigo et al. (2020b), as an efficient gradient-free ensemble-based sampler), gradient-free ALDI augmented by approximated gradient information (EGI-ALDI), gradient-free ALDI with estimated and extrapolated gradients (EGI-ALDI-extra), and the CBS sampler of Carrillo et al. (2022a). We start with a very small ensemble of size $J = 2$ and $N = 10000$. It can be observed that EGI-LS needs a larger number of ensemble members to perform well. This is due to the fact that $J = 2$ does not yield a sufficiently good approximation to the gradient. Gradient-free ALDI, EGI-ALDI and EGI-ALDI-extra are restricted to the one-dimensional affine subspace spanned by the initial ensemble and also do not sample correctly from the posterior. CBS cannot extract sufficient information from its two-point ensemble: Both the subspace property as well as the fact that (in contrast to ALDI) no implicit gradient information is

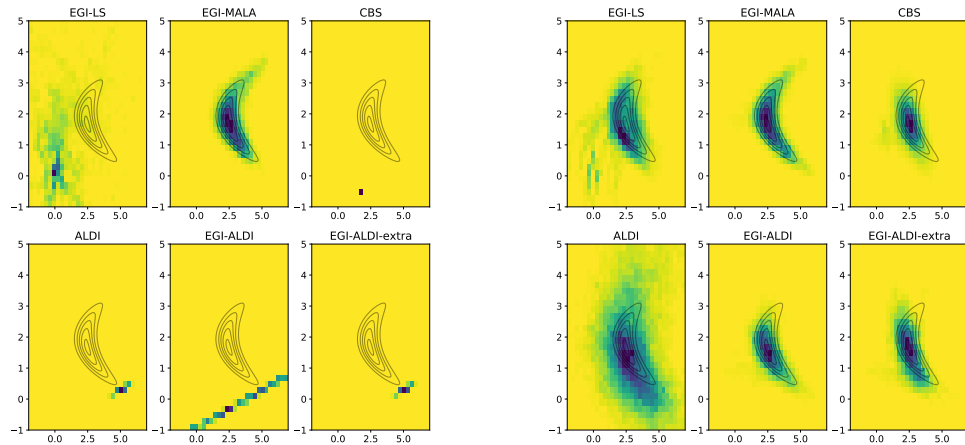
obtained leads to quick collapse to a point in the vicinity of the “better” ensemble member. EGI-MALA yields good samples: The shortcomings of EGI-LS are reigned in by the Metropolis adjustment (atrociously bad proposals due to faulty gradient approximations are rejected). For ensemble size $J = 20$ (and $N = 2000$) we see that all methods drastically improve: EGI-LS can improve its fit with the measure due to better gradient approximation (but still shows some bias), and ALDI is no longer constrained to a lower-dimensional affine subspace. Nevertheless, the forward mapping is sufficiently nonlinear that gradient-free ALDI incorporates substantial bias which strongly impacts its performance. CBS suffers in a similar way from its restricted applicability to non-Gaussian measures. EGI-ALDI and EGI-ALDI-extra profit from the gradient approximation but do not match EGI-MALA, which provides a near-perfect representation of the measure. Of course, this comes at the cost of needing to solve a larger number of linear equations as the following list (showing the amount of additional linear equations to solve per iteration) illustrates:

- EGI-LS: J linear equations (gradient approximation in each particle)
- EGI-MALA: $2 \cdot J$ linear equations (gradient approximation in each particle and each proposal)
- CBS: no additional linear equations
- ALDI: no additional linear equations
- EGI-ALDI: J linear equations (gradient approximation in each particle)
- EGI-ALDI-extra: 1 linear equation (gradient approximation only in ensemble mean)

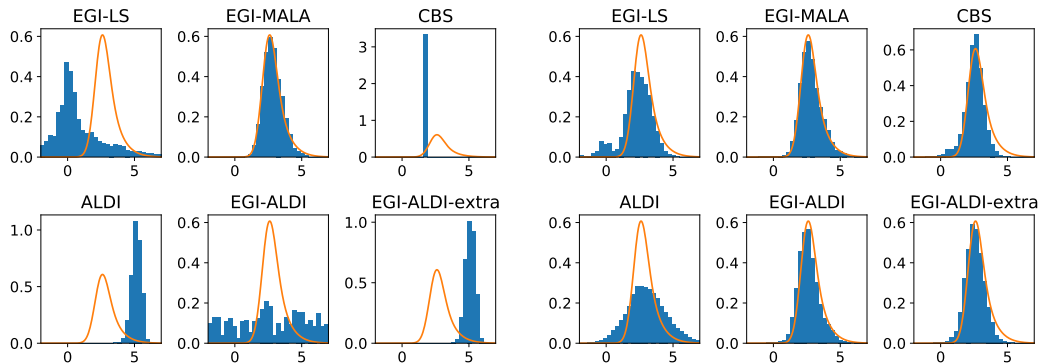
Remark 4.1. It is striking that EGI-ALDI-extra shows such a strong improvement over ALDI by use of just one additional linear equation solve per iteration, with EGI-ALDI not being much better (but much more expensive). EGI-MALA has the best performance but requires the highest number of linear equations to solve.

4.5 Discussion of results

- If the system is “almost linear”, gradient-free ALDI and CBS is much more efficient and should be preferred over EGI-LS or EGI-MALA, as there is no need to solve additional linear systems.
- On the other hand, if the ensemble size is limited (for example if evaluation of V is expensive, e.g. if it involves the numerical solution of expensive computational models), then gradient approximation is a cost-effective add-on to completely gradient-agnostic methods like CBS and Random Walk Metropolis Hastings.
- If the measure is multimodal or has a non-negligibly curved shape and gradient information is unavailable, EGI-LS and EGI-MALA can accurately approximate measures.
- If the amount of ensemble members is chosen relatively small ($J \approx d$ or less), then EGI-MALA performs much better than EGI-LS due to the Metropolis-adjustment involved.
- The extrapolation idea can be used to cut down on the amount of linear equations that needs to be solved, from $\mathcal{O}(J)$ to $\mathcal{O}(1)$.



(a) 2d histograms of samplers. $J = 2, N = 10000$ (b) 2d histograms of samplers. $J = 20, N = 2000$



(c) Marginal histogram of all six methods in comparison, where $J = 2, N = 10000$ (d) Marginal histogram of all six methods in comparison, where $J = 20, N = 2000$

Figure 9: Comparison of EGI-LS, EGI-MALA, gradient-free ALDI and EGI-ALDI. $J = 2, N = 10000$ (left column) and $J = 20, N = 4000$ (right column). Bottom row (figures 9c, 9d) show histograms of x -component of samples. The orange line marks the true marginal distribution. Code: `sampling_2d_J2.py`, `sampling_2d_J20.py`

5 Conclusion and outlook

We have described a way to turn implicit differential information from pointwise ensemble evaluation into an estimator for first (and higher order) derivatives via Ensemble-based Gradient Inference (EGI). We have presented a novel way to augment Consensus-based optimization by adding an additional drift term proportional to this approximated gradient term which can be used to find better minima and accelerates local convergence. We have also demonstrated that sampling algorithms which usually work with exact gradients can be used with inexact gradients via EGI with similar performance, but without the need for explicit gradient evaluation.

There is a lot of perspective for future work: More theoretical analysis could shed some light on the right balancing between the three terms in EGI-CBO (gradient, consensus-building, and exploratory diffusion). At this point it is still unclear under which conditions EGI-CBO can be proven to be stable and/or what its limit points are. Similarly, the heuristical trade-off between local ($\xi = 0$) and global ($\xi > 0$) EGI-CBO would need to be studied in more depth and this pertains to the sampling methods presented as well. In optimization settings where there are several similar optima one might be interested in finding all of them. A localization of CBO could help solve this issue and is subject to future work. Also for sampling methods, the analysis of convergence properties will help to guide the development of EGI variants, in particular the analysis of computational costs of EGI variants vs. accuracy improvement.

Acknowledgements

PW acknowledges support from MATH+ project EF1-19: Machine Learning Enhanced Filtering Methods for Inverse Problems.

References

- T. Back. *Evolutionary algorithms in theory and practice: evolution strategies, evolutionary programming, genetic algorithms*. Oxford University Press, 1996.
- D. Blömker, C. Schillings, P. Wacker, and S. Weissmann. Well posedness and convergence analysis of the ensemble Kalman inversion. *Inverse Problems*, 35(8):085007, 2019.
- G. Borghi, M. Herty, and L. Pareschi. An adaptive consensus based method for multi-objective optimization with uniform Pareto front approximation. *arXiv:2208.01362*, 2022.
- J. Carrillo, F. Hoffmann, A. Stuart, and U. Vaes. Consensus-based sampling. *Studies in Applied Mathematics*, 148(3):1069–1140, 2022a.
- J. A. Carrillo, Y.-P. Choi, C. Totzeck, and O. Tse. An analytical framework for consensus-based global optimization method. *Mathematical Models and Methods in Applied Sciences*, 28(06):1037–1066, 2018.
- J. A. Carrillo, S. Jin, L. Li, and Y. Zhu. A consensus-based global optimization method for high dimensional machine learning problems. *ESAIM: Control, Optimisation and Calculus of Variations*, 27:S5, 2021.

- J. A. Carrillo, F. Hoffmann, A. M. Stuart, and U. Vaes. Consensus-based sampling. *Studies in Applied Mathematics*, 148(3):1069–1140, 2022b.
- M. Fornasier, H. Huang, L. Pareschi, and P. Sünnen. Consensus-based optimization on hypersurfaces: Well-posedness and mean-field limit. *Math. Mod. Meth. Appl. Sci.*, 30(14):2725–2751, 2020.
- M. Fornasier, H. Huang, L. Pareschi, and P. Sünnen. Consensus-based optimization on the sphere: Convergence to global minimizers and machine learning. *Journal of Machine Learning Research*, 22:1–55, 2021a.
- M. Fornasier, T. Klock, and K. Riedl. Consensus-based optimization methods converge globally. *arXiv:2103.15130*, 2021b.
- M. Fornasier, T. Klock, and K. Riedl. Convergence of anisotropic consensus-based optimization in mean-field law. *Applications of Evolutionary Computation*, 13224:738–754, 2022. doi: 10.1007/978-3-031-02462-7_46.
- A. Garbuno-Inigo, F. Hoffmann, W. Li, and A. M. Stuart. Interacting langevin diffusions: Gradient structure and ensemble kalman sampler. *SIAM Journal on Applied Dynamical Systems*, 19(1):412–441, 2020a.
- A. Garbuno-Inigo, N. Nüsken, and S. Reich. Affine invariant interacting Langevin dynamics for Bayesian inference. *SIAM Journal on Applied Dynamical Systems*, 19(3):1633–1658, 2020b.
- S. Grassi and L. Pareschi. From particle swarm optimization to consensus based optimization: Stochastic modeling and mean-field limit. *Math. Mod. Meth. Appl. Sci.*, 31(08):1625–1657, 2021.
- S.-Y. Ha, M. Kang, D. Kim, J. Kim, and I. Yang. Stochastic consensus dynamics for nonconvex optimization on the stiefel manifold: Mean-field limit and convergence. *Math. Mod. Meth. Appl. Sci.*, 32(03):533–617, 2022.
- H. Huang. A note on the mean-field limit for the particle swarm optimization. *Applied Mathematics Letters*, 117:107133, 2021.
- H. Huang and J. Qiu. On the mean-field limit for the consensus-based optimization. *Mathematical Methods in the Applied Sciences*, 45(12):7814–7831, 2022.
- R. Jordan, D. Kinderlehrer, and F. Otto. The variational formulation of the Fokker–Planck equation. *SIAM Journal on Mathematical Analysis*, 29(1):1–17, 1998. URL <https://doi.org/10.1137/S0036141096303359>.
- D. Kalise, A. Sharma, and M. V. Tretyakov. Consensus based optimization via jump-diffusion stochastic differential equations. *arXiv:2205.04880*, 2022.
- K. Klamroth, M. Stiglmayr, and C. Totzeck. Consensus-based optimization for multi-objective problems: a multi-swarm approach. *in preparation*, 2022.
- N. Nüsken and S. Reich. Note on interacting Langevin diffusions: Gradient structure and ensemble Kalman sampler by Garbuno-Inigo, Hoffmann, Li and Stuart. *arXiv preprint arXiv:1908.10890*, 2019.

- R. Pinnau, C. Totzeck, O. Tse, and S. Martin. A consensus-based model for global optimization and its mean-field limit. *Mathematical Models and Methods in Applied Sciences*, 27(01):183–204, 2017.
- G. O. Roberts and R. L. Tweedie. Exponential convergence of Langevin distributions and their discrete approximations. *Bernoulli*, pages 341–363, 1996.
- C. Schillings and A. M. Stuart. Analysis of the ensemble Kalman filter for inverse problems. *SIAM Journal on Numerical Analysis*, 55(3):1264–1290, 2017.
- D. Simon. *Evolutionary optimization algorithms*. John Wiley & Sons, 2013.
- C. Totzeck. Trends in consensus-based optimization. In N. Bellomo, J. A. Carrillo, and E. Tadmor, editors, *Active Particles, Volume 3: Advances in Theory, Models, and Applications*, pages 201–226. Springer International Publishing, Cham, 2022.
- C. Totzeck and M.-T. Wolfram. Consensus-based global optimization with personal best. *Math. Biosci. Eng.*, 17(5):6026–6044, 2020. doi: 10.3934/mbe.2020320.
- P. J. van Laarhoven and E. H. Aarts. *Simulated Annealing: Theory and Applications*. Springer, 1987.
- J. Yang, G. O. Roberts, and J. S. Rosenthal. Optimal scaling of Metropolis algorithms on general target distributions. *arXiv: Computation*, 2019.